Magnetization reversal in arrays of Co rings

U. Welp,* V. K. Vlasko-Vlasov, J. M. Hiller, and N. J. Zaluzec
Materials Science Division, Argonne National Laboratory, 9700 S. Cass Avenue, Argonne, Illinois 60439, USA

V. Metlushko
Department of Electrical and Computer Engineering, University of Illinois at Chicago, 851 S. Morgan Street, Chicago, Illinois 60607-0024, USA

B. Ilic
Cornell Nanofabrication Facility, School of Applied and Engineering Physics, Cornell University, Ithaca, New York 14853, USA
(Received 7 April 2003; published 7 August 2003)

The magnetization behavior of arrays of individual and coupled Co rings has been studied using superconducting quantum interference device magnetometry, magneto-optical imaging, and Lorentz transmission and scanning transmission electron microscopy. The transition from the polarized into the vortex state of *isolated rings* is shown to occur through the motion and annihilation of head-to-head domain boundaries. The chirality of the vortex state is fixed on subsequent magnetization cycles, indicating that it is predetermined by structural imperfections of the rings. The effect of interactions between the rings has been investigated in arrays of chains of *touching rings*. For fields applied parallel to the chains rings in extended sections of the chains are found to switch simultaneously. Neighboring rings in these sections can display alternating chirality as well as the same chirality accompanied by a 180° boundary on the nodes. For fields perpendicular to the chain direction the switching occurs pairwise. This coupling introduces a broad distribution of switching fields and correspondingly a magnetization curve that is significantly broader than that for the parallel orientation.

DOI: 10.1103/PhysRevB.68.054408 PACS number(s): 75.75.+a, 75.70.Kw

I. INTRODUCTION

The magnetic properties of ferromagnetic rings have attracted considerable attention since they show unique properties that may hold great potential for technological applications such as high-density storage or magnetic random access memory (MRAM).[1] Recent studies[2–4] of Co rings with various sizes have shown that a totally flux-closed magnetic vortex structure is stable at remanence. The two chiralities of the vortex, clockwise $(-)$ and counterclockwise $(+)$, have been proposed[1] as the carriers for the stored information that could be read in a magnetoresistance-based device. Magnetic vortices have been observed in magnetic disk-shaped samples[5–11] with diameters larger than about 100 nm (depending on sample thickness and materials parameters). However, for smaller diameters the substantial exchange energy associated with the vortex core renders the vortex unstable. In ring-shaped samples the vortex core is absent, and thus stable vortex states in smaller elements—that is, at higher packing densities—appear feasible. In addition, the vortex state does not generate magneto-static stray fields, which have been shown[12–15] to influence the switching behavior in densely packed arrays of magnetic elements. Alternatively, coupling between rings can be introduced in a controlled fashion by direct contact. In this case the multiple stable magnetic states (vortices of both chiralities and fully polarized states of both signs) may generate novel properties as have been recently envisioned in quantum cellular automata.[16]

Here we present a study of the magnetization behavior of arrays consisting of Co rings with 10 μm diameter and 1 μm width (see inset in Fig. 1). Two array topologies have been investigated: a square array with 15 μm period and an array of chains of touching rings separated by 10 μm (inset, Fig. 5). The average magnetic properties of the arrays have been determined using superconducting quantum interference device (SQUID) magnetometry, whereas the magnetic patterns arising during the magnetization cycle have been imaged using a high-resolution magneto-optical imaging technique[17] and Lorentz transmission and scanning transmission electron microscopy (LTEM-LSTEM). We find that, depending on the field history, the isolated rings in the square array at remanence can be in either of two states, the vortex state or a polarized state containing domain boundaries. The transition from the polarized into the vortex state at the field H_1 occurs through the motion and annihilation of domain boundaries whereas the transition from the vortex state into the polarized state at the field H_2 involves the nucleation of domain boundaries. Averaged over a large array of rings we find a broad distribution of switching fields with the width of H_2 being significantly narrower than that of H_1. The magneto-optical images allow in a straightforward way the determination of the chirality of the vortices. We observe that on subsequent field cycles the chirality of the separated rings is fixed, indicating that the vortex chirality is predetermined by structural irregularities of the rings. This allows manufacturing a desired vortex chirality by the controlled introduction of specific shape features such as notches.[3] The magnetization process of the chains of touching rings displays a clear anisotropy depending on whether the field is applied parallel or perpendicular to the chains. For parallel field rings in extended sections of the chains are found to switch simultaneously. In these sections neighboring rings either display vortices of alternating chirality or the same chirality. In the

latter case a 180° boundary forms on the nodes. For fields perpendicular to the chain direction the switching occurs pairwise. This pair coupling introduces a broad distribution of switching fields and correspondingly a magnetization curve that is significantly broader than that for the parallel orientation.

II. EXPERIMENT

Polycrystalline Co films of 30 nm thickness were grown using *e*-beam evaporation onto SiO/Si substrates that are covered with exposed *e*-beam resist. The samples for Lorentz microscopy were grown onto 25-nm-thick Si_3N_4 windows. During film deposition the substrates were rotating in order to eliminate residual in-plane magnetic anisotropies. The ring arrays were prepared using *e*-beam lithography and a liftoff process. In the resulting structures the magnetization behavior is determined by the interplay of exchange energy and magnetostatic energy. The high-resolution magneto-optical imaging technique employed here utilizes a Bi-doped yttrium-iron-garnet sensor layer placed onto the sample for detecting the component of the magnetic stray fields that is normal to the sample surface. In contrast to magnetic-force microscopy where the stray fields of the scanning tip can modify the magnetic state of the sample[2,18] the imaging technique employed here does not interfere with the magnetic state of the sample. In the images shown below bright contrast represents strong perpendicular local fields that point out of the plane and dark contrast represents fields pointing into the plane. LTEM-LSTEM was carried out using both the AAEM VGHB503Z and the FEI TecnaiF20 instruments. The AAEM was operated at 300 kV in the Lorentz STEM mode[19] and the TenaiF20 at 200 kV in Lorentz TEM (Ref. 20) mode. For all experiments the specimen was loaded in a double-tilt stage and introduced into the microscope at near-zero-field conditions. LSTEM-LTEM observations were conducted in both instruments with the objective lens deexcited and the nominal field zeroed. Observations of magnetic domains were accomplished by judiciously tilting the samples and applying a variable vertical magnetic field using the objective lens coils, which can be varied in excitation from 0 to approximately 1 T. Typical resolution for magnetic domain imaging in LSTEM-LTEM modes was <100 nm and dynamic observation of domain motion during field-induced switching was recorded on video tape as appropriate. In the Lorentz imaging presented in this work, the magnetic domains are delineated at the domain boundaries by either white and dark Fresnel interference lines. In contrast to the magneto-optical images, which measure the normal component of the field, the Lorentz EM methods elucidate the in-plane fields of the domains.

III. RESULTS AND DISCUSSION

Figure 1 shows the magnetization curve of the square array of isolated rings for magnetic fields applied in the plane along the square diagonal. Rotation of the field in the sample plane did not reveal any anisotropy, indicating that the array behaves as an ensemble of independent rings. The magnetization curve is characterized by a substantially reduced remanent moment of about 2/3 and by a pronounced break in slope occurring slightly above the coercive field of 120 Oe as indicated by the arrow. These features can be accounted for by imaging the magnetic patterns as described below.

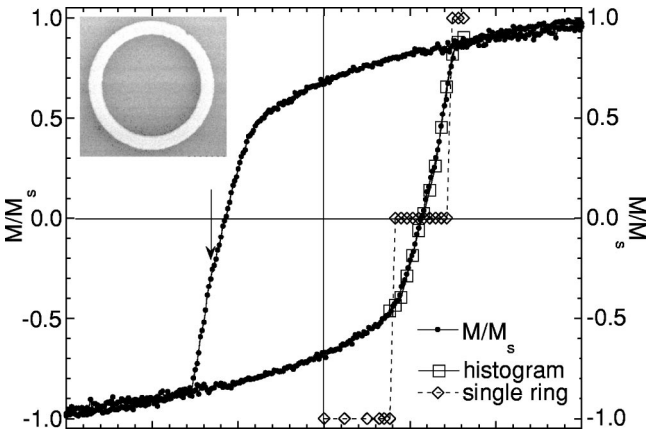

FIG. 1. Magnetization curve of the square array of isolated Co rings measured along the square diagonal. The arrow marks the break in slope of the magnetization curve (the derivative dm/dH is shown in Fig. 3 together with the histogram of switching fields). Also shown are the magnetization values calculated using the histogram. For comparison, the switching of a single ring is included. The inset shows a SEM image a single ring.

Figure 2 shows magneto-optical images of the magnetic patterns of a single ring at various stages of the magnetization process. The top row displays remanent states after initial preparation of the polarized magnetic state in a large negative field (a), after the transition into the vortex state (b), and after the transition into the new polarized state (c). The domain boundaries in the polarized states (a) and (c) are clearly seen as bright (head-to-head) and dark (tail-to-tail) spots. The Lorentz microscopy image [frame (i)] of one ring out of a chain (shown in Fig. 8) indicates that these boundaries are of vortex type. This is expected[21,22] since the width $w \approx 1$ μm of the rings is much larger than the dipolar exchange length $d = \pi\sqrt{2A/\mu_0 M_s^2} \approx 10$ nm with $A = 1.4 \times 10^{-11}$ J/m and $M_s = 1.4 \times 10^6$ A/m the exchange constant and the saturation magnetization of Co, respectively. The Lorentz microscopy image also reveals a pattern of fine striations that are oriented perpendicular to the average magnetization direction. This pattern is reminiscent of magnetic ripples that are frequently observed in the magnetization reversal of thin polycrystalline films.[23] No magneto-optic contrast is discernable in the vortex state [Fig. 2(b)] indicative for the complete flux closure. The middle row shows the corresponding in-field images. Since the external field turns the magnetic moments and thus induces magnetic charges at the ring perimeters, a magnetic contrast is also observable in the vortex state (e). This contrast is asymmetric, being stronger in the lower left section of the ring than in the upper right. The asymmetry is caused by the fact that in the lower left the magnetic moments are largely antiparallel to the field and form larger angles with the ring edge (larger magnetic charges) than in the upper right where they are aligned with the field direction. This interpretation is supported by image

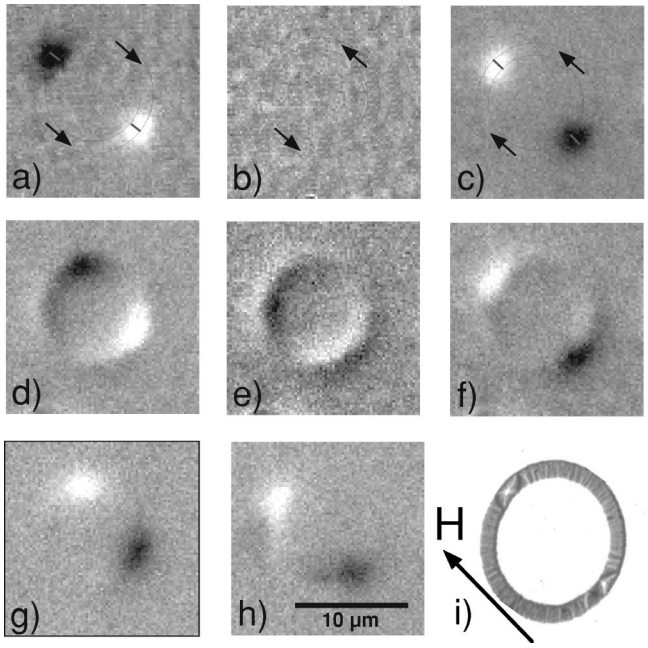

FIG. 2. Magneto-optical images of an individual ring in various magnetic states: (a) initial polarized remanent state, (b) remanent state after transition into the vortex state at 119 Oe, (c) remanent state after transition into the reversed polarized state at 133 Oe, (d) in-field image at 106 Oe, (e) in-field image at 119 Oe, (f) in-field image at 133 Oe, (g) ratio of images (e) and (d) and (h) ratio of images (f) and (e). In the top row the outline of the ring and magnetization orientations are indicated. (i) Lorentz TEM image of the center ring of the chain shown in Fig. 8 revealing the vortex structure of the head-to-head domain boundaries and the magnetic ripple. In this image the ring appears oval since the sample is tilted in the electron microscope.

(d) taken in 106 Oe just below the transition into the vortex state. The two domain boundaries have shifted towards the upper right, indicating that this section of the ring switches into the field direction by the motion and annihilation of the domain boundaries. The asymmetric field distribution seen in the in-field images of the vortex state allows for a straightforward determination of the chirality of the vortex. This is most conveniently achieved by evaluating ratios of images such as shown in frame (h) which is the ratio of images (f) (after switching into the reversed polarized state) and (e) (in the vortex state). The ratio images reveal the changes of the magnetic patterns. Frame (h) shows the changes that occur during the transition from the vortex state into the new polarized state. The domain boundaries appear, and the stray fields at the lower left disappear; i.e., this part of the ring reverses polarity. No changes occur at the upper right section of the ring since it is already polarized along the field direction. Thus the vortex in Fig. 2(e) has counterclockwise, i.e., $+$, chirality.

Even though Fig. 2 shows that individual rings display sharp transitions into the vortex state at a field H_1 and out of the vortex state at a field H_2, no corresponding features are discernable in the macroscopic magnetization curve (Fig. 1). The reason lies in the broad distribution of switching fields as shown in Fig. 3. These results, obtained by tracking the

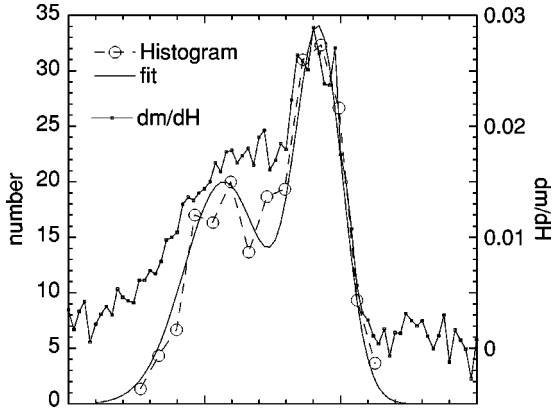

FIG. 3. Distribution of switching fields from the polarized state into the vortex state, H_1, and from the vortex state into the reversed polarized state, H_2, of the array of isolated rings. The solid line is a fit with two superimposed Gaussian distributions. On the right scale the numerical derivative dm/dH of the magnetization curve in Fig. 1 is shown.

magnetic states of 120 rings, can be described well by two Gaussian distributions representing the transitions at H_1 and H_2, respectively. The distributions are centered at $\langle H_1 \rangle = 107$ Oe and $\langle H_2 \rangle = 142$ Oe with widths of 14.5 Oe and 8.8 Oe, respectively. We note that the distribution for H_2 is significantly sharper than that of H_1. A similar observation was recently made in a magnetic force microscopy (MFM) study on arrays of Permalloy rings.[25] A possible reason lies in the different nature of the transitions at H_1 and H_2. At H_1 domain boundaries move and annihilate [see Fig. 2(d)], a process that is governed by the coercivity of domain wall motion and is thus very sensitive to microstructural details of the ring[3,4] causing the relatively broad distribution of H_1. In contrast, at H_2 the vortex annihilates through the nucleation and motion of two domain boundaries. This process requires overcoming a significantly larger energy barrier than domain wall coercivity and is not as sensitive to microstructural defects but is driven by shape anisotropy.[26]

The distribution of switching fields accounts for the break in slope of the magnetization curve as indicated by the close resemblance of the histogram and the derivative dm/dH of the magnetization curve shown in Fig. 3. In fact, the field dependence of the magnetization can be accurately recalculated from the histogram as shown in Fig. 1. For these calculations the same increment in the magnetization has been assigned to each switching event and the resulting trace has been scaled in absolute value to the initial and final magnetization values. Even though this approach neglects a small field-induced moment in the rings, the magnetization reversal is accurately reproduced. Also included is the field dependence of the magnetic state of a single ring [chosen arbitrarily in the array and marked by a circle in Fig. 4(b)]. Values of -1, 1, and 0 represent the negative- and positive-polarized state and vortex state, respectively. The transitions at H_1 and H_2 and the extended intervening vortex state are clearly seen even for rings as large as 10 μm.

In fields above 300 Oe the magnetization saturates at levels significantly higher than the remanent value (see Fig. 1).

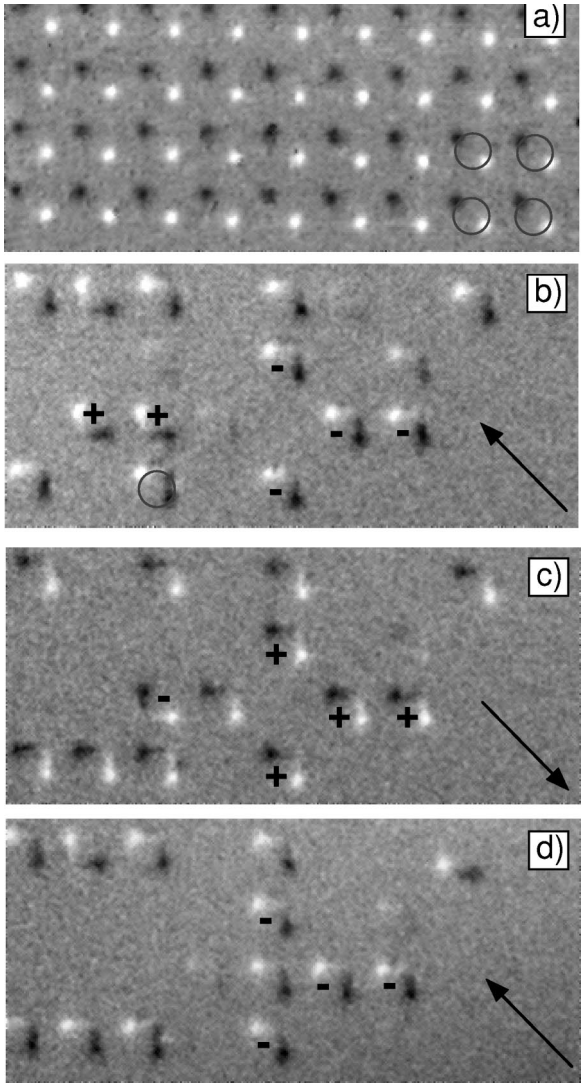

FIG. 4. Magneto-optical image of the remanent state of the square array after magnetization along the diagonal. The location of the rings is indicated by circles. Ratio images showing the transition at H_2 on repeated field cycles for field steps from 144 to 150 Oe (b), from 144 to 150 Oe (c), and from 144 to 150 Oe (d).

This reduced remanence is a consequence of the ring shape which at zero applied field induces in each ring magnetization components transverse to the measurement direction. Evaluating the circular geometry and neglecting effects due to the domain boundaries yields a reduction of the remanence by $2/\pi$ which is in good agreement with the measured value.

The chirality of the vortices is investigated in Fig. 4. Frame (a) shows the polarized remanent state. The location of the rings is indicated in the lower right. Frames (b)–(d) show ratio images displaying the transition at H_2 occurring for several rings when the absolute value of the field is increased from 144 to 150 Oe on the first positive, the first negative, and the second positive reversal. The asymmetric field distribution in the rings is clearly seen [as discussed in Fig. 2(h)], allowing the assignment of the chirality as indicated. The asymmetry is the same on each reversal, indicating that the same side of the ring switches and that the chirality is determined by defects in the rings which nucleate the initial reversal. A similar conclusion has been reached based on the analysis of Kerr hysteresis loops on Co rings.[3] Also, it has recently been shown that the chirality of vortices in disks is determined by slight deviations from the ideal circular symmetry.[27,28]

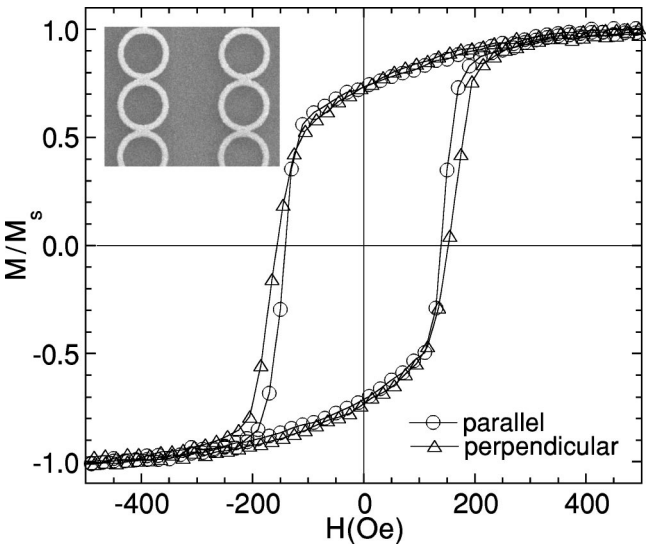

FIG. 5. Magnetization curves of the array of chains of Co rings measured in fields parallel and perpendicular to the chains. The inset shows a SEM image of the chains.

In the following, the effects of coupling between the rings are investigated on the array of chains of touching rings (inset, Fig. 5). Their magnetization curves for fields applied parallel and perpendicular to the chains are shown in Fig. 5. The switching for the parallel configuration is steeper with a reduced coercive field whereas the onset of the switching for both orientations occurs at the same field of 115 Oe. The magnetic pattern at remance after polarization parallel to the chain direction is shown in Fig. 6. Strong magnetic contrast is only visible at the ends of the chains seen along the bottom of the image. Weak magnetic contrast consisting of a pair of bright and dark spots occurs at the nodes between the rings. This type of contrast is consistent with a large degree of flux closure occurring when the oppositely charged domain boundaries in the neighboring rings are brought in close proximity. This flux closure structure consisting of a 90° domain is directly seen in the Lorentz microscopy image shown in the inset.

The magnetic patterns arising at different stages of the remagnetization of one chain in parallel fields are shown in Fig. 7. The top row displays the remanent states after the application of the reversal fields indicated in the figure caption. The bottom row [frames (f)–(h)] displays ratio images that show the changes of the magnetic structures that occur on increasing the field and that lead to the remanent states in the corresponding image in the top row. Frame (e) shows the magnetic contrast in a large applied field to illustrate the location of the rings and the weak contrast at the nodes. After the application of 142 Oe the top rings have switched into the vortex state. A pronounced dark spot marks the (now

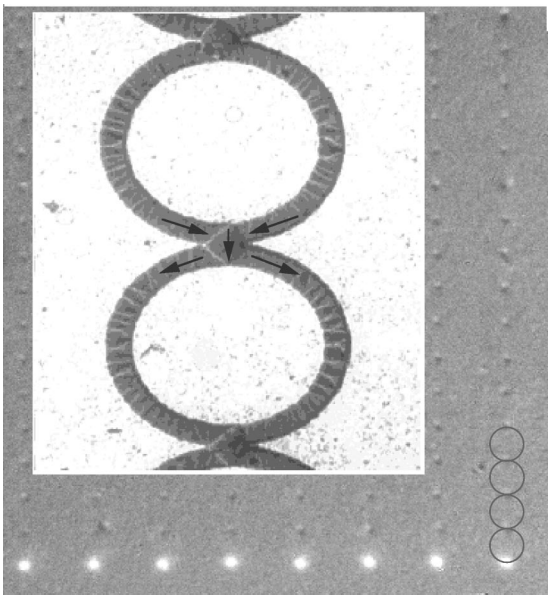

FIG. 6. Magneto-optical image of the remanent state after magnetization along the chains. The location of the rings is indicated in the lower right. The Lorentz TEM image (inset) shows the flux closure domains at the nodes and the ripple structure of the remanent state. The arrows indicate the moment directions. The rings appear elliptical since the sample is tilted along the cahin axis.

uncompensated) tail-to-tail domain boundary at the node between the switched and still-polarized rings. As shown by the meandering contrast in image (f) the chirality of vortices alternates from ring to ring, resulting in an arrangement that resembles interlocking gears. At the nodes all the magnetic moments are essentially parallel, and as a consequence the magnetic contrast at the nodes [cf. frame (b)] disappears. Increasing the field to 148 Oe switches the remainder of the chain either into the vortex state or directly into the reversed polarized state. We observe sections of the chain in which neighboring vortices have the same chirality, implying that at the nodes moments from the neighboring rings have opposite orientation and that a domain boundary forms.[24] Consequently, magnetic contrast is clearly visible at the nodes separating rings with the same chirality [cf. frame (c)]. A possible magnetic structure of the node consists of a 180° Néel boundary confined by the sample geometry. Since this structure nucleates in an applied field pointing to the top in Fig. 7, the rotation sense of the boundary is such that its core is polarized to the top. Correspondingly, the magnetic contrast at the node shows bright at the top and dark at the bottom independent of whether the boundary is located between two positive or negative vortices [see Fig. 7(c)]. An applied field of 162 Oe switches the chain into the reversed polarized state [frame (d)]. The corresponding ratio image (h) clearly shows the chirality of the rings and the location of two rings that reversed (within field steps of about 6 Oe) directly without the intermediate vortex state. We observe that during remagnetization in fields parallel to the chains the perturbation—that is, the domain boundary—propagates from node to node over extended sections of the chains. However, the length of the sections and the exact magnetic

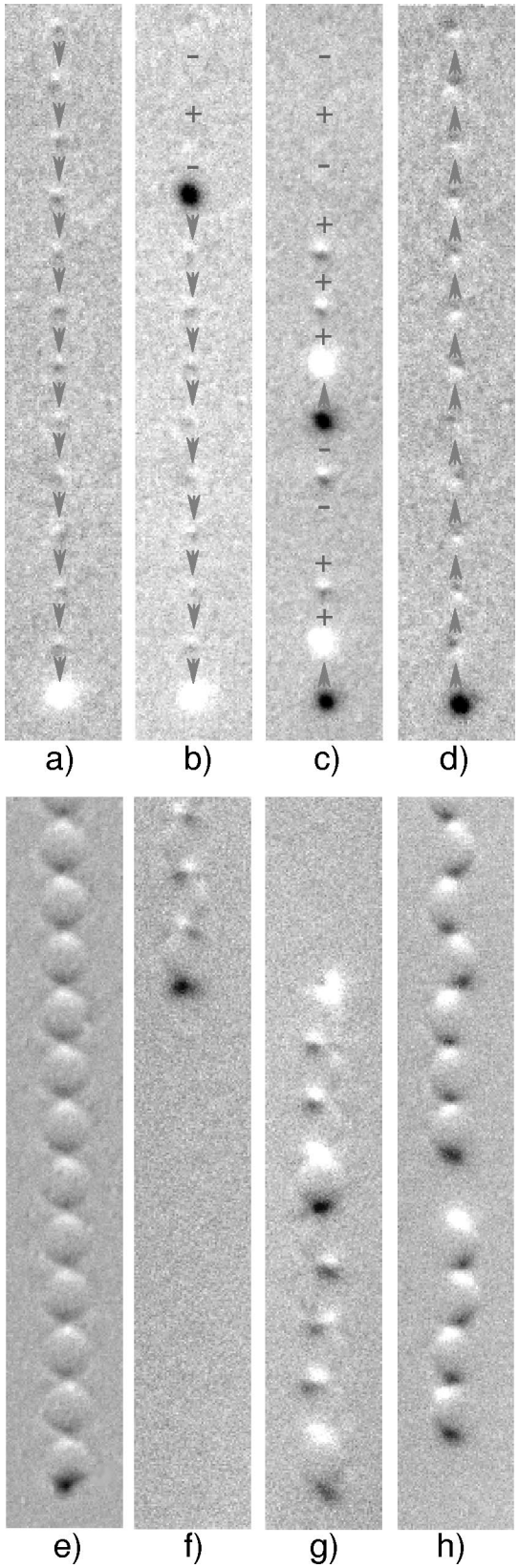

FIG. 7. Top row: remanent images (a) after initial polarization of the rings along the chain, (b) after 142 Oe, (c) after 148 Oe, and (d) after 162 Oe. Bottom row: (e) in-field image at 200 Oe; ratio of images in (f) 142 and 136 Oe, (g) 148 and 142 Oe, and (h) 162 and 156 Oe.

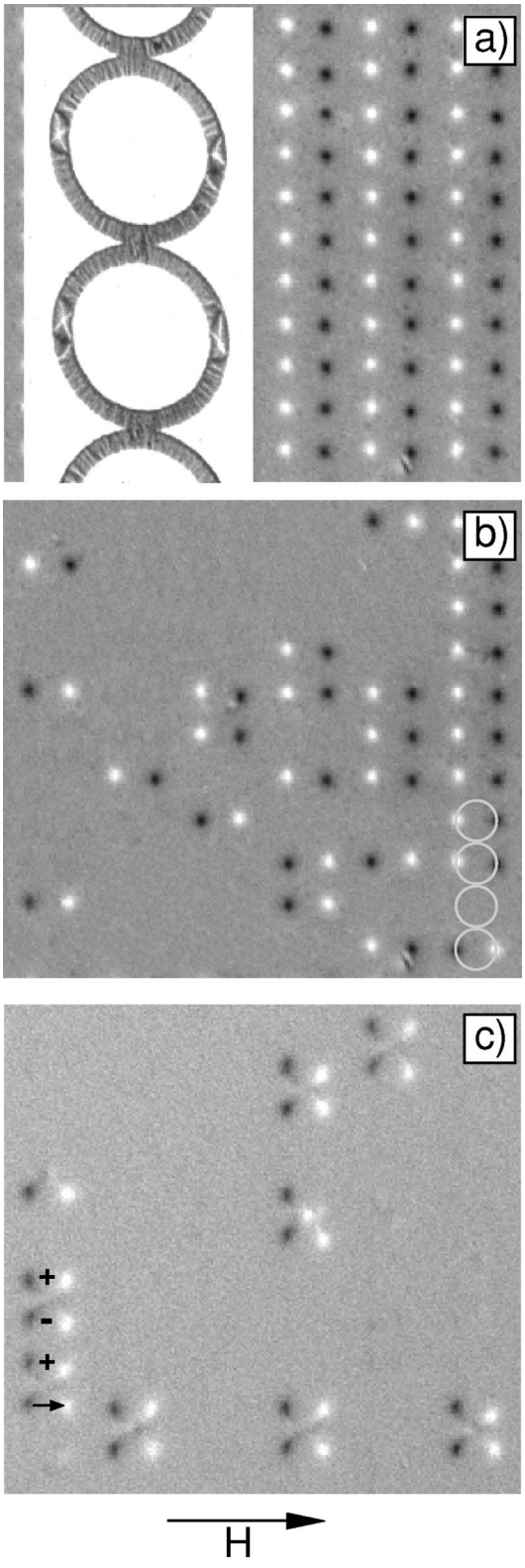

FIG. 8. Magneto-optical images of the remanent states after (a) initial polarization and (b) after 151 Oe transverse to the chains. (c) Ratio of images in 151 and 148 Oe. The Lorentz TEM image (inset) shows the formation of vortex domain boundaries and of the ripple structure. The rings in the Lorentz TEM image appear oval because the sample is tilted by $\approx 30°$ around the chain axis.

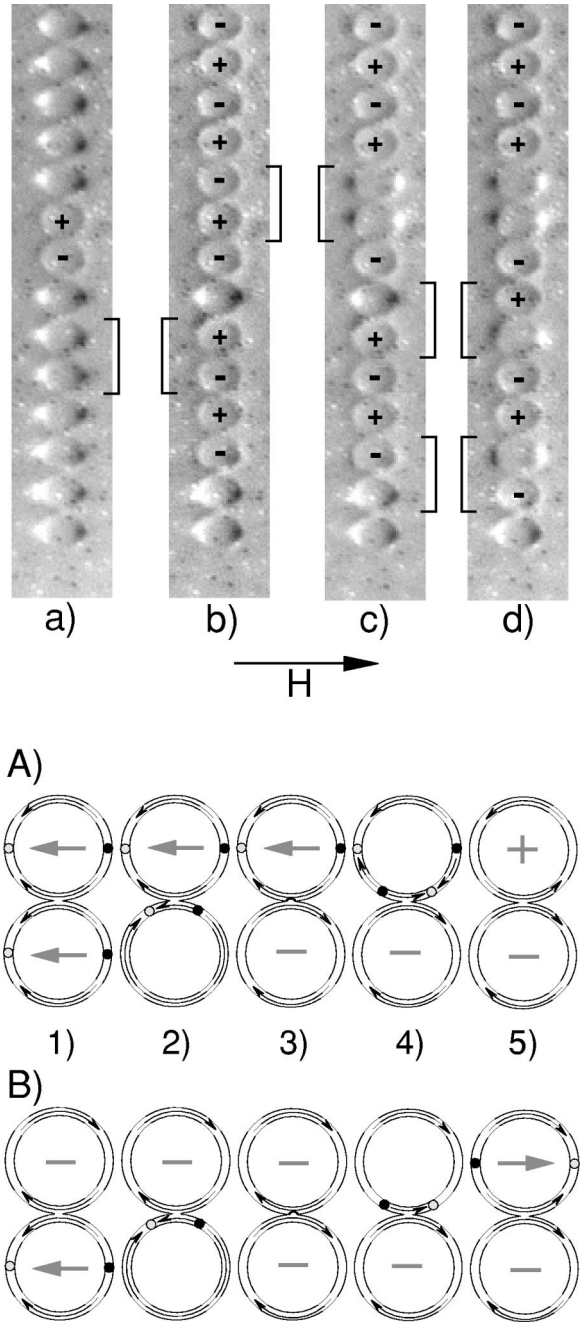

FIG. 9. Images in transverse field of (a) 11 Oe, (b) 154 Oe, (c) 157 Oe, and (d) 165 Oe. The brackets indicate pairs of rings that underwent switching. Schematics (A) and (B) outline the pair-wise switching combining rings in the same state (A) and in different states (B).

pattern that arise during reversal may vary from run to run. Short-range correlations in the switching and chirality of vortices have recently been observed in densely packed arrays of cobalt disks.[29] In this case the coupling of the magnetic states of neighboring rings is caused by fringing fields, which for closely spaced elements is not negligible.[15,30]

The magnetization behavior of the chains in transverse fields is shown in Fig. 8. Frames (a) and (b) display the initial remanent state and the remanent state after the appli-

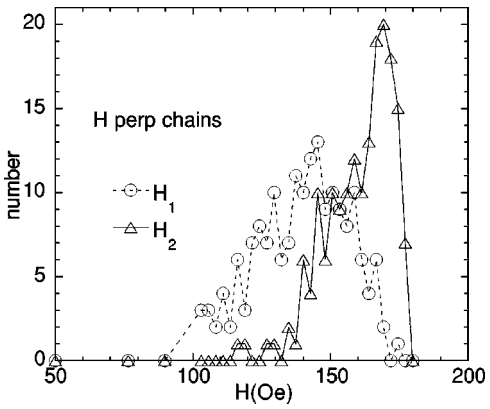

FIG. 10. Distribution of switching fields H_1 and H_2 for transverse fields.

cation of 151 Oe, respectively. The inset in (a) displays the Lorentz TEM image revealing the vortex structure of the head-to-head domain boundaries on the sides of the rings and ripple structure along the perimeter [see also Fig. 2(i)]. Rings in the vortex state (no visible contrast) coexisting with rings in the initial polarization as well as in the reversed polarization are observed in (b). The ratio image [frame (c)] showing the magnetization changes that produced the state shown in (b) reveals that rings switch in pairs. Single events are rare and likely tight to structural defects of the ring. The pairwise switching can be understood as shown in schematic (A) in Fig. 9. The transition from the polarized state into the vortex state occurs through the motion and annihilation of the two domain boundaries in one ring [see (A2)]. They can move to the top or bottom node of the ring, resulting in a vortex of positive or negative chirality. As the two boundaries annihilate a 180° boundary forms in the node connecting to the neighboring ring [see (A3)]. In contrast to the parallel field configuration where a 180° Néel boundary at the node can be stable, the transverse field promotes the motion of the boundary into the neighboring ring. The boundary splits in the node and propagates into the two branches of the ring (A4) where it annihilates the existing boundaries thus forming a vortex of opposite chirality (A5). At this point, however, the switching event stops unless a new, independent event is nucleated in neighboring rings. In contrast, in parallel field the reversal process—i.e., the motion and annihilation of the domain walls—travels from node to node, thereby remagnetizing extended sections of the chains as shown in Fig. 7.

Schematic (A) shows how two rings in the same magnetic state—i.e., polarized—switch to yield rings that have the same final state (vortices). Experimental realizations are shown in Figs. 9(a) and 9(b). In addition, two rings initially in the vortex state with their node polarized against the field direction can switch into two rings both in the reverse-polarized state as shown in Figs. 9(b) and 9(c) and highlighted by square brackets. Alternatively, rings in different magnetic states—i.e., vortex and polarized—can combine in the switching event as outlined in schematic (B). Examples for this mechanism are shown in Figs. 9(c) and 9(d). An interesting feature of these pairwise switching mechanisms is the conservation of chirality (or topological charge). The chirality can be defined as the total magnetization rotation along the ring perimeter in counterclockwise direction divided by 2π. Then the vortex states will have chirality of ± 1 and the polarized states have zero chirality. For example, both the initial and final states shown in the schematics (A) and (B) have a fixed chirality of 0 and -1, respectively. The coupled switching shown in schematic (B) has a strong effect on the distribution of switching fields. Since in this coupled event in the same applied field one ring undergoes the transition from the polarized state into the vortex state whereas the second ring undergoes the transition into the reverse-polarized state, the distributions of switching fields in the transverse geometry are broad and strongly overlapping as shown in Fig. 10. Values of H_1 extend almost to the upper bound of H_2 values. As a consequence, the magnetization curve for transverse field does not display breaks in slope as were observed for the isolated rings.

IV. CONCLUSION

In conclusion, the magnetization behavior of arrays of Co rings has been studied using magnetization measurements, magneto-optical imaging, and Lorentz TEM-STEM. Isolated Co rings on a square lattice form two stable magnetic states: a totally flux closed vortex state and a polarized state with two head-to-head domain boundaries. The transition from the polarized into the vortex state is shown to occur through the motion and annihilation of the domain boundaries. A relatively broad distribution of switching fields for the transition into the vortex state is found for the array whereas the distribution for the transition into the polarized state is significantly narrower. The chirality of the vortex state is found to be fixed on subsequent magnetization cycles, indicating that it is predetermined by structural imperfections of the rings. The effect of interactions between the rings has been investigated in arrays of chains of touching rings. For fields applied parallel to the chains, rings in extended sections of the chains are found to switch simultaneously. Neighboring rings in these sections can display alternating chirality as well as the same chirality accompanied by a 180° boundary on the nodes. For fields perpendicular to the chain direction the switching occurs pairwise and conserves the integral chirality of the rings. This coupling introduces a broad distribution of switching fields and correspondingly a magnetization curve that is significantly broader than that for the parallel orientation.

ACKNOWLEDGMENTS

This work was supported by the U.S. Department of Energy, BES, Materials Science under Contract Nos. W-31-109-ENG-38 and DE-FG02-97ER45653, and by the NSF under Contract No. ECS-0202780. The Lorentz microscopy was performed at the Electron Microscopy Center at ANL.

*Electronic address: welp@anl.gov

[1] J.-G. Zhu, Y. Zheng, and G.A. Prinz, J. Appl. Phys. **87**, 6668 (2000).
[2] S.P. Li, D. Peyrade, M. Natali, A. Lebib, Y. Chen, U. Ebels, L.D. Buda, and K. Ounadjela, Phys. Rev. Lett. **86**, 1102 (2001).
[3] M. Kläui, J. Rothman, L. Lopez-Diaz, C.A.F. Vaz, J.A.C. Bland, and Z. Cui, Appl. Phys. Lett. **78**, 3268 (2001).
[4] J. Rothman, M. Kläui, L. Lopez-Diaz, C.A.F. Vaz, A. Bleloch, J.A.C. Bland, Z. Cui, and R. Speaks, Phys. Rev. Lett. **86**, 1098 (2001).
[5] M. Hehn, K. Ounadjela, J.-P. Bucher, F. Rousseaux, D. Decanini, B. Bartenlian, and C. Chappert, Science **272**, 1782 (1996).
[6] R.P. Cowburn, D.K. Koltsov, A.O. Adeyeye, M.E. Welland, and D.M. Tricker, Phys. Rev. Lett. **83**, 1042 (1999).
[7] A. Fernandez and C. Cerjan, J. Appl. Phys. **87**, 1395 (2000).
[8] T. Shinjo, T. Okuno, R. Hassdorf, K. Shigeto, and T. Ono, Science **289**, 930 (2000).
[9] M. Schneider, H. Hoffmann, and J. Zweck, Appl. Phys. Lett. **77**, 2909 (2000).
[10] J. Raabe, R. Pulwey, R. Sattler, T. Schweinbock, J. Zweck, and D. Weiss, J. Appl. Phys. **88**, 4437 (2000).
[11] V. Novosad, K.Yu. Guslienko, H. Shima, Y. Otani, K. Fukamichi, N. Kikuchi, O. Kitakami, and Y. Shimada, IEEE Trans. Magn. **37**, 2088 (2001).
[12] K.J. Kirk, J.N. Chapman, and C.D.W. Wilkinson, Appl. Phys. Lett. **71**, 539 (1997).
[13] R.E. Dunin-Borkowski, M.R. McCartney, B. Kardynal, and D.J. Smith, J. Appl. Phys. **84**, 374 (1998).
[14] X.B. Xu, A. Hirohata, L. Lopez-Diaz, H.T. Leung, M. Tselepi, S.M. Gardiner, W.Y. Lee, J.A.C. Bland, F. Rousseaux, E. Cambaril, and H. Launois, J. Appl. Phys. **87**, 7019 (2000).
[15] V. Novosad, K.Yu. Guslienko, H. Shima, Y. Otani, S.G. Kim, K. Fukamichi, N. Kikuchi, O. Kitakami, and Y. Shimada, Phys. Rev. B **65**, 060402 (2002).
[16] R.P. Cowburn and M.E. Welland, Science **287**, 5146 (2000).
[17] V.K. Vlasko-Vlasov, U. Welp, J.S. Jiang, D.J. Miller, G.W. Crabtree, and S.D. Bader, Phys. Rev. Lett. **86**, 4386 (2001).
[18] U. Welp, V.K. Vlasko-Vlasov, G.W. Crabtree, C. Thompson, V. Metlushko, and B. Ilic, Appl. Phys. Lett. **79**, 1315 (2000).
[19] N.J. Zaluzec, in *Microscopy and Microanalysis 2001*, edited by W. Bailey (Springer-Verlag, Berlin, 2001), Vol. 7 Supl. 2, pp. 222–224.
[20] L. Reimer, *Transmission Electron Microscopy*, Springer Series in Optical Sciences Vol. 36, edited by P. Hawkes (Springer-Verlag, Berlin, 1989), p. 260.
[21] R.D. McMichael and M.J. Donahue, IEEE Trans. Magn. **33**, 4167 (1997).
[22] M.-F. Lai, C.-R. Chang, J.C. Wu, Z.-H. Wei, J.H. Kuo, and J.-Y. Lai, IEEE Trans. Magn. **38**, 2550 (2002).
[23] A. Hubert and R. Schäfer, *Magnetic Domains* (Springer-Verlag, Berlin, 1998).
[24] A. Hirohata, C.C. Yao, H.T. Leung, Y.B. Xu, C.M. Guertler, and J.A.C. Bland, IEEE Trans. Magn. **36**, 3068 (2000).
[25] X. Zhu, P. Grütter, V. Metlushko, and B. Ilic (unpublished).
[26] L. Lopez-Diaz, J. Rothman, M. Kläui, and J.A.C. Bland, IEEE Trans. Magn. **36**, 3155 (2000).
[27] M. Schneider, H. Hoffmann, and J. Zweck, Appl. Phys. Lett. **79**, 3113 (2001).
[28] M. Grimsditch, P. Vavassori, V. Novosad, V. Metlushko, H. Shima, Y. Otani, and K. Fukamichi, Phys. Rev. B **65**, 172419 (2002).
[29] M. Natali, I.L. Prejbeanu, A. Lebib, L.D. Buda, K. Ounadjela, and Y. Chen, Phys. Rev. Lett. **88**, 157203 (2002).
[30] K.Yu. Guslienko, V. Novosad, Y. Otani, H. Shima, and K. Fukamichi, Phys. Rev. B **65**, 024414 (2002).